Rovibrational Energies of $^{13}C^{16}O_2$ Determined with Kilohertz Accuracy

Published as part of The Journal of Physical Chemistry A *virtual special issue* "Xueming Yang Festschrift".

Zi-Tan Zhang, Fang-Hui Cao, Shan Jiang, An-Wen Liu,* Yan Tan, Y. R. Sun, and Shui-Ming Hu

Read Online

ACCESS | Metrics & More | Article Recommendations | SI Supporting Information

ABSTRACT: Accurate spectroscopic data of carbon dioxide are widely used in many important applications, such as carbon monitoring missions. Here, we present comb-locked cavity ring-down saturation spectroscopy of the second most abundant isotopologue of CO_2, $^{13}C^{16}O_2$. We determined the positions of 88 lines in three vibrational bands in the 1.6 μm region, 30011e/ 30012e/30013e−00001e, with an accuracy of a few kHz. Based on the analysis of combination differences, we obtained for the first time the ground-state rotational energies with kHz accuracy. We also provide a set of hybrid line positions for 150 $^{13}C^{16}O_2$ transitions. The rotational energies ($J < 50$) in the 30013e vibrational state can be fitted by a set of rotational and centrifugal constants with deviations within a few kHz, indicating that the 30013e state is free of perturbations. These precise isotopic line positions will be utilized to improve the Hamiltonian model and quantitative remote sensing of carbon dioxide. Moreover, they will help to track changes in the carbon source and sink through isotopic analysis.
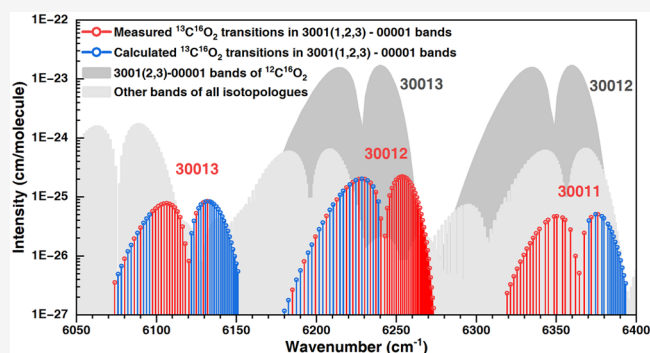
INTRODUCTION

Carbon dioxide, the most important anthropogenic greenhouse gas, is the focus of several satellite missions such as OCO-2/ OCO-3[1,2] (NASA), GOSAT/GOSAT-2[3,4] (JAXA), TanSat[5] (CAS), and the upcoming MicroCarb[6] (CNES) and CO2M[7] (ESA) missions, as well as ground-based networks such as TCCON,[8] to quantitatively determine its atmospheric mole fraction. As a principal constituent, the molecule is also important in studies of the atmospheres of Venus and Mars.[9,10] To obtain accurate CO_2 information from observational data, high-precision line parameters of CO_2 in the infrared region, especially in the 1.6 μm region where the commonly used 3001(2,3)e−00001e bands of $^{12}C^{16}O_2$ are located, are increasingly required for various missions and remote sensing programs. In this region, high-precision line parameters of $^{12}C^{16}O_2$ have been reported in the past decade.[11−18] However, to improve the accuracy of CO_2 remote sensing and emerging infrared absorption spectroscopy for determining stable carbon isotope ratios,[19] high-precision line parameters of other isotopologues are still required. Line parameters of $^{13}C^{16}O_2$, the second most abundant isotopologue with a terrestrial abundance of 1.1%, are of particular interest. The absorption lines of $^{13}C^{16}O_2$ in the same region overlap strongly with the 3001(2,3)e−00001e bands of $^{12}C^{16}O_2$, as shown in Figure 1. The frequencies and intensities of $^{13}C^{16}O_2$ lines in this region are currently best determined through theoretical calcula-

tions.[20−22] However, the uncertainties have not met the requirements of retrieval algorithms.[23,24]

Here, we present Lamb-dip measurements of the 30011e/ 30012e/30013e−00001e bands of $^{13}C^{16}O_2$ by comb-locked cavity ring-down spectroscopy near 1.6 μm. The positions of 88 lines were determined with an accuracy of a few kHz. Through spectroscopic analysis and combination difference calculations, we obtained ground-state rotational energy levels with kHz accuracy for the first time. A set of hybrid line positions of 150 $^{13}C^{16}O_2$ transitions near 1.6 μm is also provided. These high-precision line parameters will provide a benchmark for improving effective Hamiltonian models and will benefit quantitative remote sensing of atmospheric carbon dioxide and stable carbon isotope analysis.
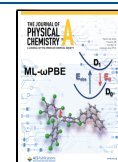
EXPERIMENTAL SECTION

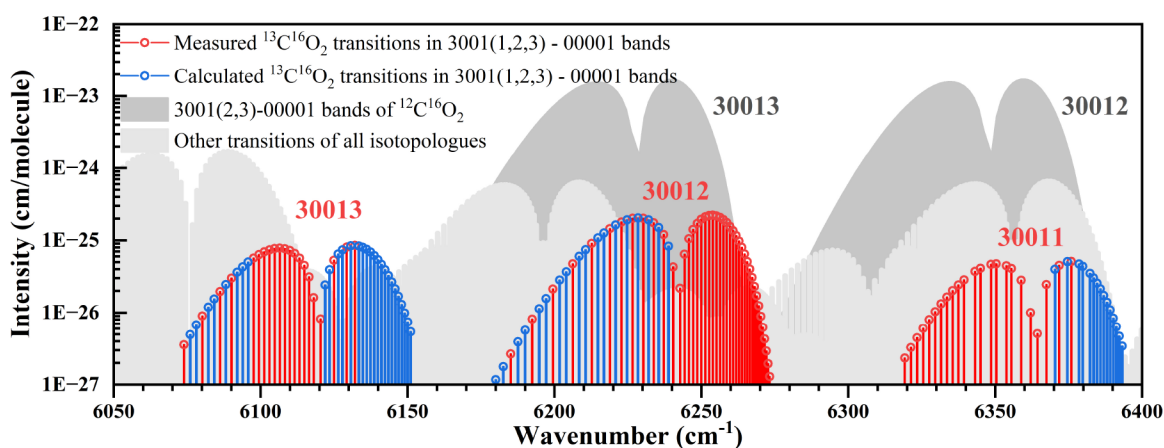The configuration of the comb-locked cavity ring-down spectroscopy setup is illustrated in Figure 2, which is similar

Figure 1. Overview of the 3001(1,2,3)e−00001e bands of $^{13}C^{16}O_2$ as provided by the HITRAN2020[25] database. Transitions presently measured (red) and calculated (blue) in this work are highlighted.
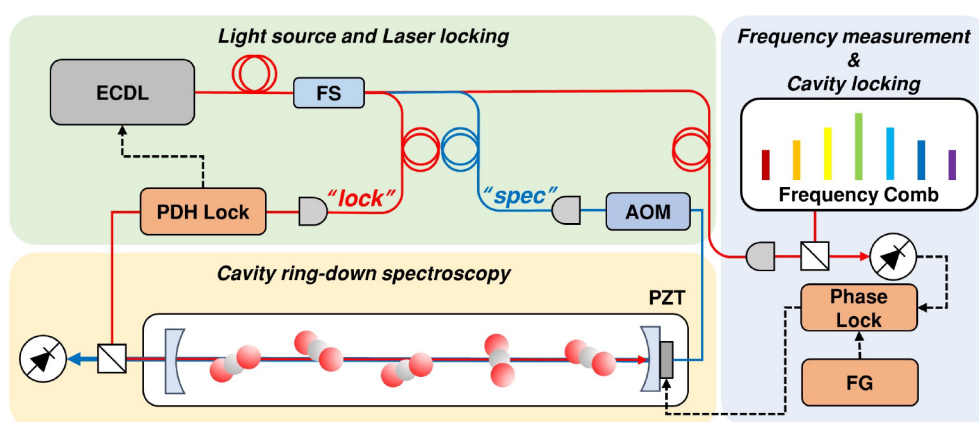

Figure 2. Experimental setup of the comb-locked cavity ring-down spectroscopy. ECDL: external-cavity diode laser. FS: fiber splitter. PDH: Pound-Drever-Hall. AOM: acoustic-optical modulator. PZT: piezoelectric actuator. FG: function generator.

to the setup used in our previous studies.[16,26] A tunable external cavity diode laser (ECDL, Toptica DL Pro) is used as the light source, which delivers two beams with different polarizations, labeled by "spec" and "lock", respectively. The "lock" beam is locked to an optical cavity by the Pound−Drever−Hall (PDH) method. The cavity consists of a pair of high-reflective (HR) mirrors ($R \approx 99.997\%$ at $1.55-1.65\ \mu m$), and one of the mirrors is mounted on a piezoelectric actuator (PZT). The mirrors are placed at two ends of a cylindrical cavity made of invar. The distance between the two mirrors is 108 cm, leading to a free spectral range (FSR) of 138.8 MHz, a finesse of 105 000, and a mode width of about 1.3 kHz. The cavity temperature is stabilized at 298.15 K, and the variation is less than 10 mK. The cavity length is stabilized by the PZT, which is controlled by a feedback servo based on the beat signal between the "lock" beam and an optical frequency comb. The comb's repetition frequency (f_{rep}) and carrier envelope offset frequency (f_{ceo}) are locked to precise radiofrequency sources, both referenced to a Global Positioning System (GPS) disciplined rubidium clock. The "spec" beam, frequency shifted by an acoustic-optic modulator (AOM) of exactly 1 FSR, is coupled into the cavity from the other end of the cavity and used to generate the ring-down signal. The "spec" beam and the return light of the "lock" beam are separated by a combination of polarizing waveplates (not shown in the figure) and a polarizing beam splitter (PBS) cube. The "spec" beam

power is adjustable from 0.6 to 4.6 mW, resulting in the intracavity power of 3.5−25 W, to maintain a proper saturation for strong and weak lines. The AOM also serves as a beam chopper that is triggered by an external rectangle wave to shut off the "spec" beam and initiate ring-down events. Since we have locked the probe laser to the cavity and locked the cavity to one of the teeth of the frequency comb, the "spec" beam is always in resonance with the cavity, and the cavity length is stabilized during the ring-down event. In this way, we do not need to dither the piezo actuator to match the laser with a cavity mode and avoid the Doppler effect due to the moving mirror.[27] The ring-down curve is fitted to an exponential decay function by the Levenberg−Marquart method to derive decay time τ. The sample absorption coefficient (α) is determined from the change of the cavity decay time: $\alpha = 1/c\tau - 1/c\tau_0$, where c is the speed of light, and τ and τ_0 are the decay times of the cavity with and without sample, respectively. The minimum detectable absorption coefficient reached about $6.5 \times 10^{-12}\ cm^{-1}$ at an average time of 1 s. Lamb-dip spectra can be measured by tuning the reference frequency (f_B) of the phase-lock circuit, which is generated by a function generator (FG). Therefore, the frequency of the "spec" beam can be determined by

$$\nu = N \times f_{rep} + f_{ceo} + f_B + f_{AOM} \tag{1}$$
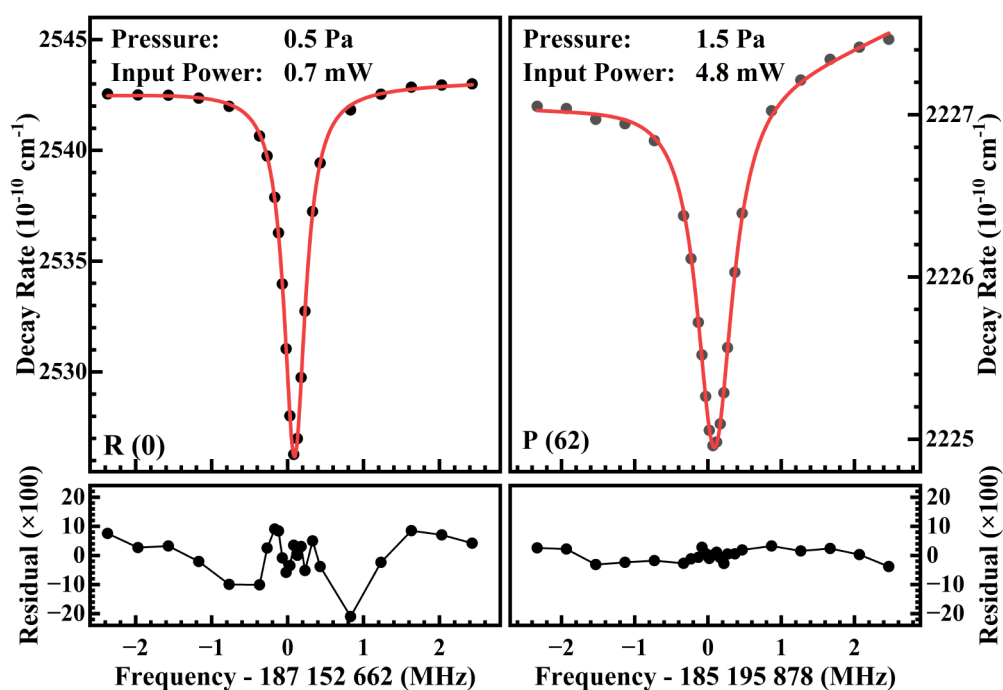
where f_{AOM} is the AOM driving frequency.

Figure 3. Lamb-dip spectra of the R(0) and P(62) lines in the 30012e−00001e band of $^{13}CO_2$ recorded under different experimental conditions. Red lines represent fitted curves by using a Lorentzian profile and a linear baseline. Fitting residuals are shown in the lower panels.

RESULTS AND DISCUSSION

Line Positions and the Uncertainty Budget. In this work, we measured 88 lines in the 3001(1,2,3)e−00001e bands of $^{13}C^{16}O_2$. According to the HITRAN2020 database,[25] their intensities vary in the range 7.5×10^{-28} to 2.2×10^{-25} cm molecule^{-1}. A ^{13}C enriched carbon dioxide sample (from Wuhan Niuruide Gas Company) with stated $^{13}CO_2$ abundance >99% was used. Lamb-dip spectra were recorded under pressures in the range 0.3−2.5 Pa depending on the intensities of the transitions. Figure 3 shows spectra of the R(0) and P(62) lines in the 30012e−00001e band recorded under different experimental conditions, respectively. Lorentzian functions with linear baselines were used to fit the Lamb-dips, and the simulated spectra are shown as solid lines in the top panels of Figure 3, along with the fitting residuals illustrated in the bottom panels of Figure 3.

Here, the P(2) line in the 30012e−00001e band is used as an example for the uncertainty analysis. Various sources of uncertainty for the transition frequency are discussed below and summarized in Table. 1. In Lamb-dip measurements, the

Table 1. Uncertainty Budget for the Position of the P(2) Line in the 30012e−00001e Band of $^{13}CO_2$ (Unit: kHz)

Source	Frequency	Uncertainty
Statistical	187 082 468 105.3	0.06
Comb frequency		0.4
Locking servo		0.1
AOM frequency		<0.05
Pressure shift		0.3
Power shift		0.3
Exponential fit range		0.04
Line profile asymmetry		0.3
Second-order doppler	+0.17	0.01
Total	187 082 468 105.5	0.6

ring-down signals no longer decrease exponentially with time. A nonexponential model has been proposed to obtain more reliable Lamb-dip profiles.[28] However, we can still use simple exponential functions to fit the ring-down curve in studies focusing on transition frequencies,[16,29,30] despite the fact that this treatment may distort the line profile of the Lamp-dip.[31] One reason is that the saturation parameter is still small in this work ($S \ll 1$), and another is that the symmetry of the Lamb-dip should not shift the line center. As shown in Figure 4, when we used different start voltages (while the end voltages remain the same) in fitting the ring-down curves, we could see a change in the Lamb-dip depths, but the change of center frequencies is within the experimental uncertainty. We did not see a dramatic systematic variation due to the fitting strategy reported by Bielska et al.[32] Figure 4(c) shows a standard deviation of 0.04 kHz and is used as an estimate of the systematic uncertainty from this effect.

We measured the Lamb-dips at different sample pressures of 0.3, 0.5, 0.8, 1.2, and 1.5 Pa under the same input laser power of 0.64 mW. Line centers derived from these spectra are given in Figure 5(a), which show no pressure dependence. A linear fit gave a slope of 0.03 ± 0.87 kHz/Pa. Note that the collision-induced pressure shift of this line obtained from Doppler-limited measurements was −1.4 kHz/Pa.[33] The phenomenon that the pressure shift in line centers obtained in Lamb-dip measurements vanishes at low pressures has also been reported in our previous studies[16,17] of $^{12}CO_2$. The mechanism has also been discussed in studies of some other molecules.[34,35] The deviation of 0.3 kHz between the line centers obtained at different pressures is used as the systematic uncertainty due to the pressure shift. We also measured the Lamb-dips of the P(2) line at 0.8 Pa and different input laser powers of 0.64, 0.94, 1.5, and 2.95 mW. The intracavity laser power was estimated according to the signal obtained from the photodiode and the transmittance of the cavity.[28,36] The intracavity power is calculated to be 3.2, 4.6, 7.4, and 14.6 W, respectively,
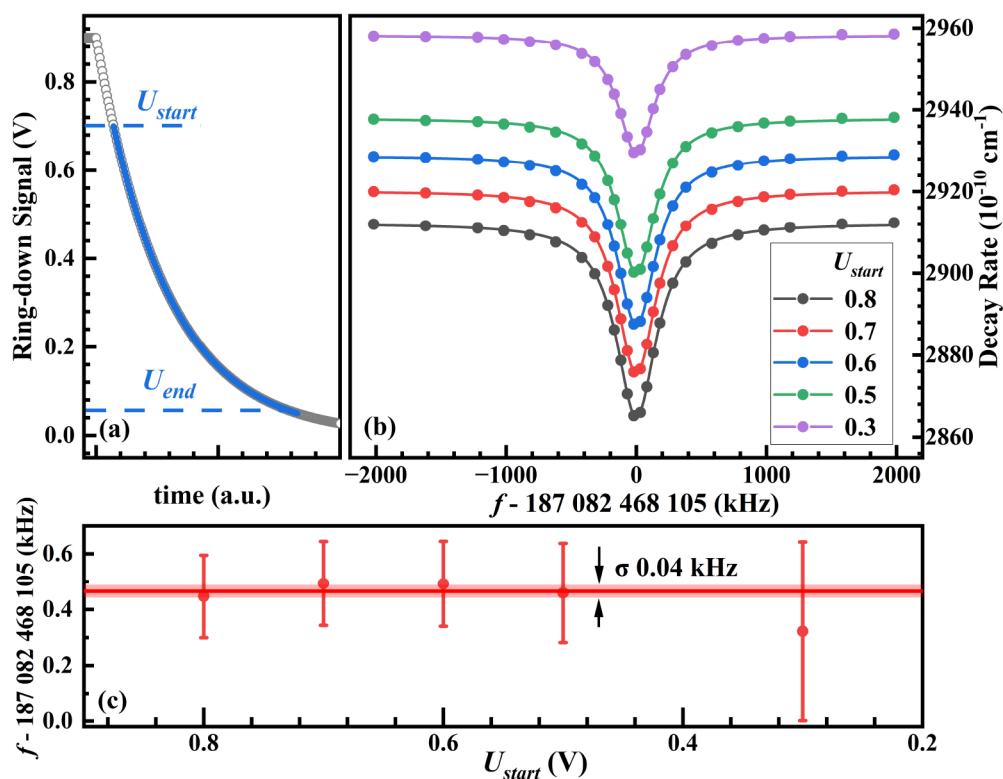
Figure 4. (a) Fitting a ring-down curve within a given set of start (U_{start}) and end (U_{end}) voltage signal ranges. (b) Lamb-dip spectra of the P(2) line in the 30012e−00001e band obtained with different U_{start} (while U_{end} remains the same). Spectra were shifted for a better illustration. The sample pressure was 0.8 Pa, and the input laser power was 1.5 mW. (c) Positions of the P(2) line obtained with different U_{start}.
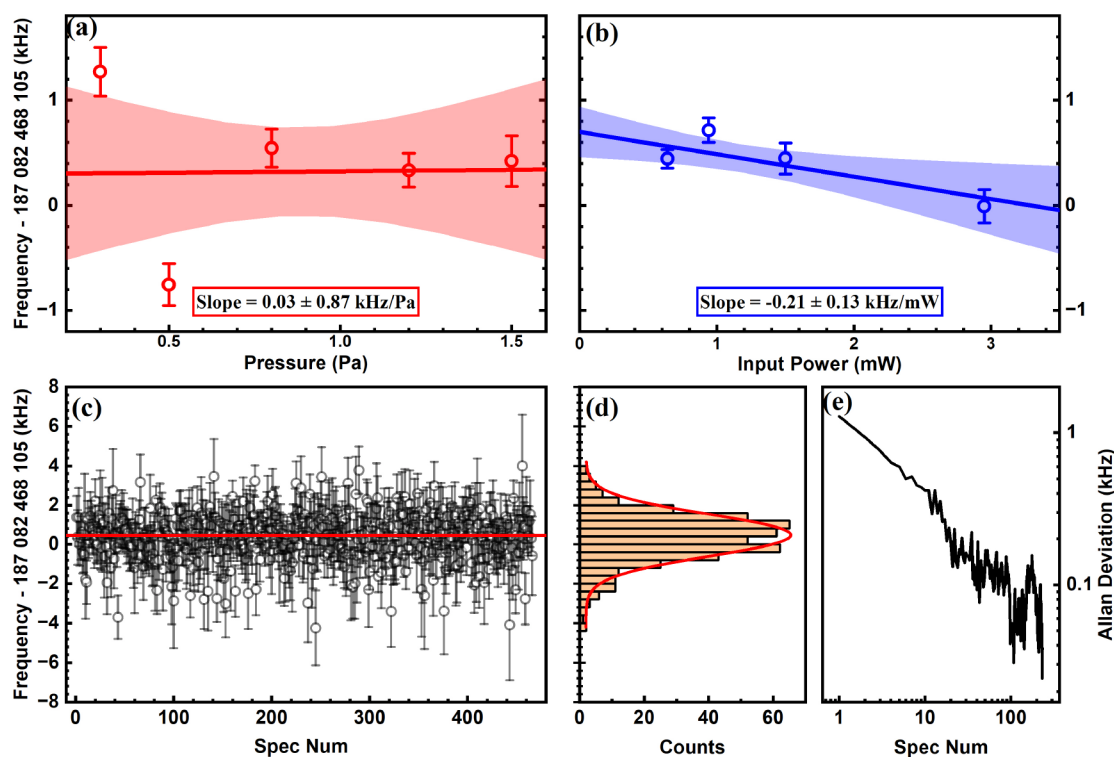
Figure 5. (a) Line centers measured at different sample pressures (0.3−1.5 Pa) with input laser power of 0.7 mW. The red line and band indicate the linear fitting result with 1σ confidence. (b) Line centers measured at different input laser powers (0.6−3 mW) with the same sample pressure of 0.8 Pa. The blue line and band indicate the linear fitting result with 1σ confidence. (c) Line centers obtained from each CRDS scan (466 in total). (d) Histogram plot of the line centers in 0.4 kHz bins with an overlaid normal distribution. (e) Allan deviation of the line centers.

Table 2. Frequencies of the Transitions in the 3001(1,2,3)e−00001e Bands of $^{13}CO_2$ Determined in This Work with Their 1σ Uncertainties (Unit: kHz)

Line	Freq	Ns[a]	P[b]	Line	Freq	Ns[a]	P[b]
			30011e−00001e				
R(0)	190 799 777 279.3(11)	528	0.5	P(28)	190 049 805 963.1(22)	70	1.0
R(4)	190 890 672 027.4(13)	54	0.5	P(30)	189 992 382 212.8(20)	60	1.0
R(10)	191 021 241 519.5(06)	143	0.5	P(32)	189 934 259 773.7(08)	58	1.0
R(16)	191 144 926 559.1(08)	52	0.5	P(34)	189 875 447 361.9(13)	62	1.0
P(2)	190 729 583 309.4(10)	246	0.5	P(36)	189 815 953 960.1(15)	100	1.0
P(6)	190 633 299 069.6(11)	181	1.0	P(38)	189 755 788 698.3(14)	100	1.0
P(10)	190 533 951 351.8(08)	26	0.5	P(40)	189 694 960 673.1(24)	100	2.5
P(12)	190 483 135 559.0(14)	60	1.0	P(42)	189 633 478 720.3(24)	140	2.5
P(16)	190 379 238 808.9(08)	26	0.5	P(44)	189 571 351 068.8(28)	100	2.5
P(18)	190 326 167 003.4(09)	120	1.0	P(46)	189 508 584 854.1(34)	100	2.5
P(22)	190 217 791 559.1(16)	100	1.0	P(48)	189 445 185 380.0(28)	400	2.5
P(24)	190 162 524 357.8(13)	60	1.0				
			30012e−00001e				
R(0)	187 152 662 074.3(07)	102	0.5	R(44)	187 912 156 388.0(07)	52	0.5
R(2)	187 198 143 171.3(06)	52	0.5	R(46)	187 934 880 987.6(07)	51	0.5
R(4)	187 242 571 937.7(06)	50	0.5	R(48)	187 956 608 779.4(11)	53	0.5
R(6)	187 285 948 406.9(06)	60	0.5	R(50)	187 977 345 420.1(13)	60	0.5
R(8)	187 328 272 941.7(06)	50	0.5	R(52)	187 997 097 092.6(08)	80	1.5
R(10)	187 369 546 236.4(06)	60	0.5	R(54)	188 015 870 624.8(13)	59	1.5
R(12)	187 409 769 270.5(06)	86	0.5	R(56)	188 033 673 625.1(14)	100	1.5
R(14)	187 448 943 312.4(06)	60	0.5	R(58)	188 050 514 635.5(20)	200	1.5
R(16)	187 487 069 871.6(06)	62	0.5	R(60)	188 066 403 392.8(25)	146	1.5
R(18)	187 524 150 694.3(06)	60	0.5	P(2)	187 082 468 105.5(06)	466	0.3−1.5
R(20)	187 560 187 723.1(06)	53	0.5	P(6)	186 985 198 980.2(06)	50	0.5
R(22)	187 595 183 099.3(06)	60	0.5	P(10)	186 883 737 873.3(06)	50	0.5
R(24)	187 629 139 125.9(06)	50	0.5	P(14	186 778 101 243.6(06)	50	0.5
R(26)	187 662 058 279.8(06)	53	0.5	P(18)	186 668 310 313.4(06)	50	0.5
R(28)	187 693 943 194.0(06)	50	0.5	P(22)	186 554 390 332.3(06)	51	0.5
R(30)	187 724 796 674.1(06)	50	0.5	P(26)	186 436 369 869.0(06)	54	0.5
R(32)	187 754 621 730.6(06)	50	0.5	P(32)	186 251 720 134.7(06)	78	0.5
R(34)	187 783 421 711.6(06)	54	0.5	P(38)	186 058 034 912.1(06)	51	0.5
R(36)	187 811 201 333.0(06)	50	0.5	P(44)	185 855 432 163.2(08)	60	0.5
R(38)	187 837 935 797.8(06)	51	0.5	P(50)	185 644 080 186.5(08)	80	1.5
R(40)	187 863 695 616.4(06)	50	0.5	P(56)	185 424 152 360.9(19)	63	1.5
R(42)	187 888 429 711.6(06)	50	0.5	P(62)	185 195 878 089.3(21)	100	1.5
			30013e−00001e				
R(0)	183 484 826 360.5(08)	70	0.8	P(16)	183 068 171 005.0(10)	100	1.2
R(6)	183 620 922 670.0(06)	100	0.8	P(18)	183 016 118 170.1(10)	110	1.2
R(12)	183 751 247 352.5(06)	100	0.8	P(20)	182 963 417 199.1(07)	100	1.2
R(16)	183 834 877 727.7(06)	59	0.8	P(22)	182 910 063 984.6(11)	100	1.2
P(2)	183 414 632 389.9(08)	110	1.2	P(24)	182 856 053 922.4(07)	100	1.2
P(4)	183 367 044 053.0(12)	100	1.2	P(26)	182 801 381 954.7(09)	100	1.2
P(6)	183 318 822 003.3(13)	104	1.2	P(34)	182 575 958 433.5(06)	73	0.8
P(8)	183 269 965 779.4(07)	100	1.2	P(38)	182 459 112 366.8(10)	60	0.8
P(10)	183 220 474 377.1(07)	109	1.2	P(44)	182 278 506 105.7(07)	60	0.8
P(12)	183 170 346 249.7(11)	100	1.2	P(50)	182 091 294 074.6(12)	87	0.8
P(14)	183 119 579 328.(18)	110	1.2				

[a]Number of measured spectra. [b]Experimental pressure in Pa.

corresponding to a saturation parameter of 0.16, 0.24, 0.38, and 0.75 at the beginning of the ring-down events. Note that the values of saturation power used here are calculated by the line width retrieved from spectra with simple exponential ring-down treatment, which may result in deviations from the saturated cavity ring-down treatment.[37] Line centers obtained with different laser powers are shown in Figure 5(b). We found very little dependence of the line center on the laser power. We applied a linear fit and obtained the center at the zero-power

limit, which has a 0.3 kHz difference from the average line center. Therefore, we used the average value of the line centers, and the value of 0.3 kHz is taken for the systematic uncertainty due to the power shift, which may come from saturation-induced line profile distortion, as we mentioned above. In total, 466 line centers are obtained from all of the recorded spectra, as shown in Figure 5(c), together with the histogram shown in Figure 5(d). The average line center for the P(2) transition is

Table 3. Fitted Spectroscopic Parameters for 00001e, 3001(1,2,3)e Vibrational States of $^{13}C^{16}O_2$ (Unit: MHz)

|	00001e (ref 40)	00001e	30011e	30012e	30013e
G_v			190 776 571.67824(55)	187 129 525.26490(23)	183 461 586.93433(36)
B_v	11 699.01868(45)	11 699.0185604(67)	11 602.7115087(52)	11 567.5753840(13)	11 619.7226400(31)
$D_v \times 10^3$	3.99561(28)	3.9960333(44)	2.540936(12)	3.122633(02)	5.423200(10)
$H_v \times 10^9$	0.296(43)	0.40682(81)	24.188(10)	−70.99005(83)	30.9100(46)
$L_v \times 10^{12}$			−17.6299(25)	8.38775(12)	0.1314(10)
J_{max}	72	61	47	61	49
N		21	23	44	21
RMS	1.38	0.0013	0.51	3.81	0.0017
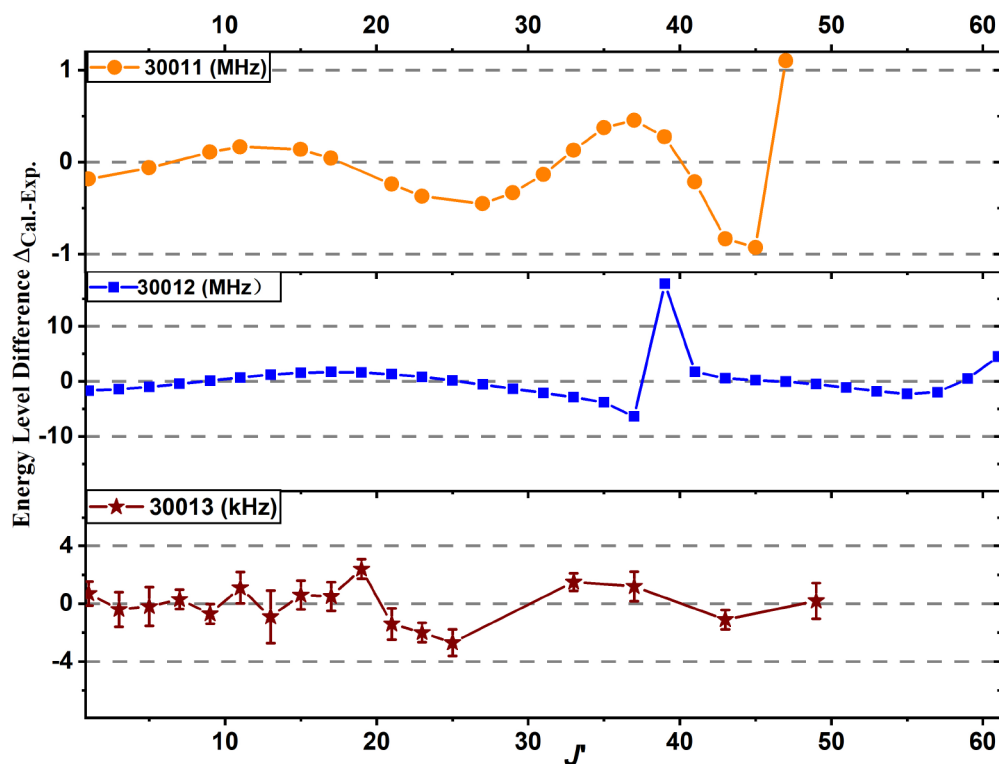
Figure 6. Energy level difference $\Delta_{cal-exp} = E_{cal} - E_{exp}$ between those calculated rotational energy derived from the spectroscopic parameters and the experimental value versus the rotational quantum number J'. Note that the vertical axis units are MHz in the upper and middle panels but kHz in the lowest panel.

187 082 468 105.3 kHz. The Allan deviation of the line centers over the number of spectra is shown in Figure 5(e).

The frequency comb contributed an uncertainty of 0.4 kHz due to the drift of 2×10^{-12} from the GPS-disciplined rubidium clock. The frequency shift due to the bias in the cavity locking servo is estimated to be about 0.1 kHz, including the drift in the PDH lock and the fluctuation in the phase-lock loop, estimated from the Allan deviation of the beat frequency between the comb and the "lock" light. The uncertainty of the radiofrequency driving the AOM due to room temperature variation is estimated to be less than 50 Hz. According to the root-mean-square velocity of 406 m/s of the $^{13}C^{16}O_2$ molecule at 298 K, the second-order Doppler shift is calculated to be 0.17 kHz with an uncertainty of less than 10 Hz. The AC Stark shift is estimated to be within a few tens of Hz, which was neglected in this work. The $^{13}C^{16}O_2$ has a hyperfine structure due to the presence of the ^{13}C atom, which has been observed in previous rotational spectra of ^{13}CO.[38] The hyperfine splitting was not resolved in our measurements, but it could broaden the line and lead to some asymmetry in the line profile. This asymmetry will result in a difference between the

fitting center and the centroid of the hyperfine transitions. By estimating the asymmetry of the residuals obtained by fitting the spectra with a Lorentzian function, we gave an uncertainty of 0.3 kHz for the P(2) line. Taking into account all the corrections and uncertainties given above, we determined the center of the P(2) line to be 187 082 468 105.5 ± 0.6 kHz.

In total, we obtained the frequencies together with uncertainties of 88 lines in the 3001(1,2,3)e−00001e bands. They are listed in Table 2, including the number of measured spectra and the experimental pressure for each line.

Spectroscopic Analysis and Comparison to Literature. For an isolated vibrational state, the vibration−rotation energy levels can be reproduced with a simple model:

$$E(J) = G_v + B_v J(J+1) - D_v J^2(J+1)^2 + H_v J^3(J+1)^3 + L_v J^4(J+1)^4 + \cdots \tag{2}$$

where G_v is the vibrational term and B_v, D_v, H_v, and L_v are rotational and centrifugal distortion constants. $^{13}C^{16}O_2$, as a symmetric molecule similar to $^{12}C^{16}O_2$, has no microwave absorption. In addition, its line positions have yet to be
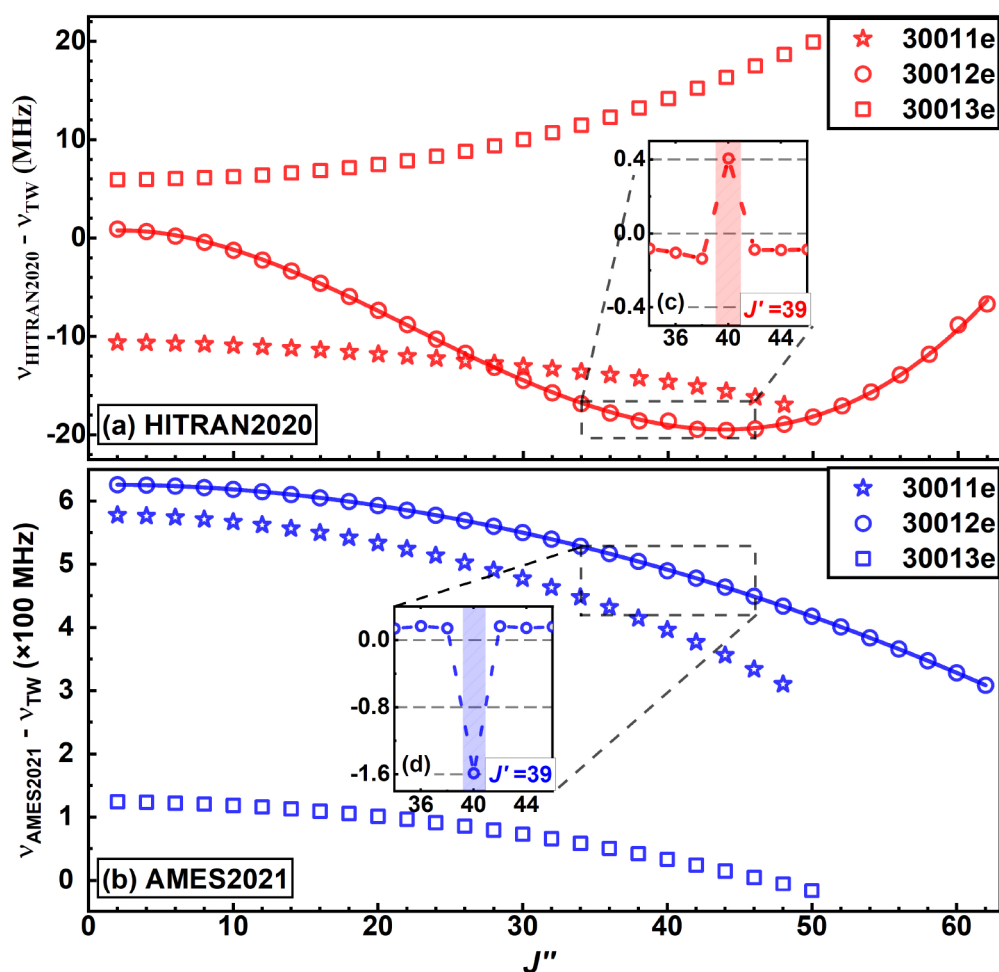
Figure 7. Comparison between the transition frequencies reported in HITRAN2020 (a)[25] and AMES2021 (b),[22] with the values obtained in this work versus J'' for P-branches of 30011e (stars), 30012e (circles), and 30013e (squares) cold bands. Residuals from a polynomial fit of the line positions around $J' = 39$ in the 30012e−00001e band are depicted in the insets.

determined with sub-MHz accuracy for transitions from the ground vibrational state. As a result, the ground state energies of $^{13}C^{16}O_2$ have not been reproduced with uncertainties at the kHz levels as those[15,16,39] of the main isotopologue $^{12}C^{16}O_2$. Twenty-one ground combination differences, $\Delta E(J') = R(J' - 1) - P(J' + 1)$, where J' is the rotational quantum number of the upper energy level, were obtained from 88 line positions in the 3001(1,2,3)e−00001e bands. They were used to retrieve a new set of ground state spectroscopic constants of $^{13}C^{16}O_2$ with a fit RMS (root-mean-square) of 1.3 kHz. The method is similar to the one we applied[16] to $^{12}C^{16}O_2$. Compared to the value of 1.38 MHz reported by Miller et al.,[40] the result improved by 3 orders of magnitude. The new set of ground-state spectroscopic constants listed in Table 3 allows us to reproduce all experimental ground-state combination differences obtained in this work within the respective 3σ combined experimental uncertainties.

By fitting 88 transition frequencies using the ground state parameters to the values determined above, we derived rovibrational spectroscopic parameters for 3001(1,2,3)e states, and they are listed in Table 3. The parameters can reproduce the line positions in the 30013e−00001e band within 3σ experimental uncertainties, as shown in the lower panel of Figure 6 (stars), indicating that the 30013e state can be considered as a very well isolated vibrational state for $J < 50$.

However, the RMS deviations reach 0.5 and 3.8 MHz for the 30011e−00001e and 30012e−00001e bands, respectively, which are hundreds of times the experimental uncertainty. This indicates that the simple model (eq 2) is not sufficiently accurate for the line positions for the 30011e and 30012e states. Based on the effective Hamiltonian model, the Carbon Dioxide Spectroscopic Databank (CDSD) group[20,41] identified the interaction mechanism from experimental line shifts and anomalous intensities. For example, the 30012e state has an anharmonic resonance interaction with the 14411e state crossing at $J = 39$ and a Coriolis resonance interaction with the 33301e state crossing at $J = 83$. The residuals of the fit plotted in the middle panel of Figure 6 (squares) clearly show that the rotational energy levels of the 30012e states are perturbed around $J = 39$. Meanwhile, we can also see that the rotational energies ($J \leq 47$) in the 30011e state (circles) are perturbed by about 1 MHz.

Taking into account perturbations to the 3001(1,2)e states, we provide a hybrid set of line positions of 150 $^{13}C^{16}O_2$ transitions in the 1564−1646 nm region as Supporting Information, which was constructed as follows.

(i) Transitions in the 30011e−00001e band: Frequencies of 23 transitions are experimental values. The calculated values were retrieved by the equation $\nu_{R(J)}^{calc} = \nu_{P(J+2)}^{exp} + E(J + 2) - E(J)$ for rest transitions in the R branch, where

$E(J + 2)$ and $E(J)$ are the calculated ground state energies.

(ii) Transitions in the 30012e−00001e band: Line positions were composed with the experimental values in the R branch, the calculated values in the P branch retrieved by the equation $\nu_{P(J)}^{calc} = \nu_{R(J-2)}^{exp} + E(J - 2) - E(J)$.

(iii) Transitions in the 30013e−00001e band: Line positions were given as calculated values with the spectroscopic parameters of 00001e and 30013e vibrational states listed in Table 3.

The frequencies in the P-branch of three bands are listed in the Supporting Information are compared with the values in different databases (Figure 7), including HITRAN2020 derived from CDSD and AMES2021. The deviations are between −20 and +20 MHz for HITRAN2020 (Figure 7a). They are not only more than 20 times larger than those of the $^{12}C^{16}O_2$ isotopologue[16,17] but also larger than the difference shown in Figure 6. The comparison with AMES2021[22] shows differences of hundreds of MHz (Figure 7b). Both HITRAN2020 and AMES2021 deviations show a strong J'' dependence for the transitions in three bands. A third-order polynomial function can reproduce the deviations with tens of kHz residuals in the 3001(1,3)e−00001e bands but leaves jumps of +0.4 and −1.6 MHz at $J' = 39$ in the 30012e band for CDSD (Figure 7c) and AMES2021 (Figure 7d), respectively. The very accurate line positions obtained in this work not only are complementary to the frequency standards in this region but also may be useful to refine the parameters of the effective Hamiltonian model for better line position predictions of the $^{13}C^{16}O_2$ isotopologue.

CONCLUSIONS

In summary, we have performed Lamb-dip measurements of the 3001(1,2,3)e−00001e bands for $^{13}C^{16}O_2$ using comb-locked cavity ring-down spectroscopy. In the measurements, both the probe laser and the optical cavity are stabilized and precisely controlled, allowing us to achieve kHz accuracy for all of the measured 88 line centers. By fitting 21 ground combination differences (with J' up to 61) from the measured transitions in the 3001(1,2,3)e−00001e bands, we obtained the ground state spectroscopic constants of $^{13}C^{16}O_2$ with uncertainties at the kHz level for the first time. The fitted spectroscopic constants of the 30013e vibrational states allow reproducing the rovibrational energy levels ($J \leq 49$) with an RMS deviation of 1.7 kHz, indicating that the vibrational state is well isolated. Meanwhile, the RMS values for the 3001(1,2)e states are hundreds of times of experimental uncertainties, indicating perturbations in these two states. Compared with line positions in different databases, HITRAN2020 derived from CDSD and AMES2021, the differences show strong J'' dependence for the transitions in all three bands. Our accurate line positions could be used to increase the accuracy of other transition frequencies by applying the Ritz principle to refine the effective Hamiltonian model.[42] The result can also help advance accurate remote sensing and isotope ratio determination.

ASSOCIATED CONTENT

Supporting Information

The Supporting Information is available free of charge at https://pubs.acs.org/doi/10.1021/acs.jpca.4c00697.

A hybrid set of line positions of 150 $^{13}C^{16}O_2$ transitions in the 1564−1646 nm region (PDF)

AUTHOR INFORMATION

Corresponding Author

An-Wen Liu − State Key Laboratory of Molecular Reaction Dynamics, Department of Chemical Physics, University of Science and Technology of China, Hefei 230026, China; Hefei National Laboratory, University of Science and Technology of China, Hefei 230088, China; orcid.org/0000-0001-9835-3530; Email: awliu@ustc.edu.cn

Authors

Zi-Tan Zhang − Hefei National Research Center for Physical Sciences at Microscale, University of Science and Technology of China, Hefei 230026, China

Fang-Hui Cao − State Key Laboratory of Molecular Reaction Dynamics, Department of Chemical Physics, University of Science and Technology of China, Hefei 230026, China

Shan Jiang − State Key Laboratory of Molecular Reaction Dynamics, Department of Chemical Physics, University of Science and Technology of China, Hefei 230026, China

Yan Tan − Hefei National Research Center for Physical Sciences at Microscale, University of Science and Technology of China, Hefei 230026, China; orcid.org/0000-0003-3073-3152

Y. R. Sun − Institute of Advanced Science Facilities, Shenzhen 518107, China

Shui-Ming Hu − State Key Laboratory of Molecular Reaction Dynamics, Department of Chemical Physics, University of Science and Technology of China, Hefei 230026, China; Hefei National Laboratory, University of Science and Technology of China, Hefei 230088, China; orcid.org/0000-0002-1565-8468

Complete contact information is available at:
https://pubs.acs.org/10.1021/acs.jpca.4c00697

Notes
The authors declare no competing financial interest.

REFERENCES

(1) Eldering, A.; Wennberg, P.; Crisp, D.; Schimel, D.; Gunson, M.; Chatterjee, A.; Liu, J.; Schwandner, F.; Sun, Y.; O'dell, C.; et al. The Orbiting Carbon Observatory-2 early science investigations of regional carbon dioxide fluxes. Science 2017, 358, No. eaam5745.

(2) Eldering, A.; Taylor, T. E.; O'Dell, C. W.; Pavlick, R. The OCO-3 mission: measurement objectives and expected performance based on 1 year of simulated data. Atmospheric Measurement Techniques 2019, 12, 2341−2370.

(3) Yokota, T.; Yoshida, Y.; Eguchi, N.; Ota, Y.; Tanaka, T.; Watanabe, H.; Maksyutov, S. Global Concentrations of CO_2 and CH_4 Retrieved from GOSAT: First Preliminary Results. SOLA 2009, 5, 160−163.

(4) Imasu, R.; Matsunaga, T.; Nakajima, M.; Yoshida, Y.; Shiomi, K.; Morino, I.; Saitoh, N.; Niwa, Y.; Someya, Y.; Oishi, Y.; et al. Greenhouse gases Observing SATellite 2 (GOSAT-2): mission overview. Progress in Earth and Planetary Science 2023, 10, 33.

(5) Liu, Y.; Wang, J.; Yao, L.; Chen, X.; Cai, Z.; Yang, D.; Yin, Z.; Gu, S.; Tian, L.; Lu, N.; et al. The TanSat mission: preliminary global observations. *Science Bulletin* **2018**, *63*, 1200−1207.

(6) Cansot, E.; Pistre, L.; Castelnau, M.; Landiech, P.; Georges, L.; Gaeremynck, Y.; Bernard, P. MicroCarb instrument, overview and first results. *Proc. SPIE* **2023**, *12777*, No. 3127774.

(7) Sierk, B.; Fernandez, V.; Bézy, J.-L.; Meijer, Y.; Durand, Y.; Courrèges-Lacoste, G. B.; Pachot, C.; Löscher, A.; Nett, H.; Minoglou, K. The Copernicus CO2M mission for monitoring anthropogenic carbon dioxide emissions from space. *Proc. SPIE* **2021**, *11852M*, No. 118523M.

(8) Wunch, D.; Toon, G. C.; Blavier, J.-F. L.; Washenfelder, R. A.; Notholt, J.; Connor, B. J.; Griffith, D. W.; Sherlock, V.; Wennberg, P. O. The total carbon column observing network. *Philosophical Transactions of the Royal Society A: Mathematical, Physical and Engineering Sciences* **2011**, *369*, 2087−2112.

(9) Hu, R.; Kass, D. M.; Ehlmann, B. L.; Yung, Y. L. Tracing the fate of carbon and the atmospheric evolution of Mars. *Nat. Commun.* **2015**, *6*, No. 10003.

(10) Snels, M.; Stefani, S.; Grassi, D.; Piccioni, G.; Adriani, A. Carbon dioxide opacity of the Venus' atmosphere. *Planetary and Space Science* **2014**, *103*, 347−354.

(11) Devi, V. M.; Benner, D. C.; Sung, K.; Brown, L. R.; Crawford, T. J.; Miller, C. E.; Drouin, B. J.; Payne, V. H.; Yu, S.; Smith, M. A. H.; et al. Line parameters including temperature dependences of self-and air-broadened line shapes of $^{12}C^{16}O_2$: 1.6-μm region. *Journal of Quantitative Spectroscopy and Radiative Transfer* **2016**, *177*, 117−144.

(12) Birk, M.; Röske, C.; Wagner, G. High accuracy CO_2 Fourier transform measurements in the range 6000−7000 cm^{-1}. *Journal of Quantitative Spectroscopy and Radiative Transfer* **2021**, *272*, No. 107791.

(13) Mondelain, D.; Campargue, A.; Fleurbaey, H.; Kassi, S.; Vasilchenko, S. CRDS measurements of air-broadened lines in the 1.6 μm band of $^{12}CO_2$: Line shape parameters with their temperature dependence. *Journal of Quantitative Spectroscopy and Radiative Transfer* **2022**, *288*, No. 108267.

(14) Truong, G.-W.; Long, D. A.; Cygan, A.; Lisak, D.; van Zee, R. D.; Hodges, J. T. Comb-linked, cavity ring-down spectroscopy for measurements of molecular transition frequencies at the kHz-level. *J. Chem. Phys.* **2013**, *138*, No. 094201.

(15) Reed, Z.; Drouin, B.; Long, D. A.; Hodges, J. T. Molecular transition frequencies of CO_2 near 1.6 μm with kHz-level uncertainties. *Journal of Quantitative Spectroscopy and Radiative Transfer* **2021**, *271*, No. 107681.

(16) Wu, H.; Hu, C.-L.; Wang, J.; Sun, Y. R.; Tan, Y.; Liu, A.-W.; Hu, S.-M. A well-isolated vibrational state of CO_2 verified by near-infrared saturated spectroscopy with kHz accuracy. *Phys. Chem. Chem. Phys.* **2020**, *22*, 2841−2848.

(17) Tan, Y.; Xu, Y.-R.; Hua, T.-P.; Liu, A.-W.; Wang, J.; Sun, Y.; Hu, S.-M. Cavity-enhanced saturated absorption spectroscopy of the (30012)-(00001) band of $^{12}C^{16}O_2$. *J. Chem. Phys.* **2022**, *156*, No. 044201.

(18) Jiang, S.; Tan, Y.; Liu, A.-W.; Xiao-guo, Z.; Hu, S.-M. Saturated Cavity Ring-Down Spectroscopy of $^{12}C^{16}O_2$ near 1.57 μm. *Chinese Journal of Chemical Physics* **2024**, *37*, 13−18.

(19) Fleisher, A. J.; Yi, H.; Srivastava, A.; Polyansky, O. L.; Zobov, N. F.; Hodges, J. T. Absolute $^{13}C/^{12}C$ isotope amount ratio for Vienna PeeDee Belemnite from infrared absorption spectroscopy. *Nat. Phys.* **2021**, *17*, 889−893.

(20) Tashkun, S.; Perevalov, V.; Gamache, R.; Lamouroux, J. CDSD-296, high-resolution carbon dioxide spectroscopic databank: An update. *Journal of Quantitative Spectroscopy and Radiative Transfer* **2019**, *228*, 124−131.

(21) Zak, E. J.; Tennyson, J.; Polyansky, O. L.; Lodi, L.; Zobov, N. F.; Tashkun, S. A.; Perevalov, V. I. Room temperature line lists for CO_2 symmetric isotopologues with ab initio computed intensities. *Journal of Quantitative Spectroscopy and Radiative Transfer* **2017**, *189*, 267−280.

(22) Huang, X.; Schwenke, D. W.; Freedman, R. S.; Lee, T. J. Ames-2021 CO_2 dipole moment surface and IR line lists: Toward 0.1% uncertainty for CO_2 IR intensities. *J. Phys. Chem. A* **2022**, *126*, 5940−5964.

(23) Miller, C.; Crisp, D.; DeCola, P.; Olsen, S.; Randerson, J.; Michalak, A.; Alkhaled, A.; Rayner, P.; Jacob, D. J.; Suntharalingam, P.; et al. Precision requirements for space-based X_{CO_2} data. *Journal of Geophysical Research: Atmospheres* **2007**, *112*, D10.

(24) Oyafuso, F.; Payne, V. H.; Drouin, B. J.; Devi, V. M.; Benner, D. C.; Sung, K.; Yu, S.; Gordon, I. E.; Kochanov, R.; Tan, Y.; et al. High accuracy absorption coefficients for the Orbiting Carbon Observatory-2 (OCO-2) mission: Validation of updated carbon dioxide cross-sections using atmospheric spectra. *Journal of Quantitative Spectroscopy and Radiative Transfer* **2017**, *203*, 213−223.

(25) Gordon, I. E.; Rothman, L. S.; Hargreaves, R.; Hashemi, R.; Karlovets, E. V.; Skinner, F.; Conway, E. K.; Hill, C.; Kochanov, R. V.; Tan, Y.; et al. The HITRAN2020 molecular spectroscopic database. *Journal of quantitative spectroscopy and radiative transfer* **2022**, *277*, No. 107949.

(26) Wang, J.; Sun, Y.; Tao, L.-G.; Liu, A.-W.; Hua, T.-P.; Meng, F.; Hu, S.-M. Comb-locked cavity ring-down saturation spectroscopy. *Rev. Sci. Instrum.* **2017**, *88*, No. 043108.

(27) Lee, J. Y.; Hahn, J. W. Theoretical investigation on the intracavity Doppler effect in continuous wave swept-cavity ringdown spectroscopy. *Appl. Phys. B: Laser Opt.* **2004**, *79*, 371−378.

(28) Giusfredi, G.; Bartalini, S.; Borri, S.; Cancio, P.; Galli, I.; Mazzotti, D.; De Natale, P. Saturated-absorption cavity ring-down spectroscopy. *Phys. Rev. Lett.* **2010**, *104*, No. 110801.

(29) Reed, Z.; Long, D.; Fleurbaey, H.; Hodges, J. SI-traceable molecular transition frequency measurements at the 10^{-12} relative uncertainty level. *Optica* **2020**, *7*, 1209−1220.

(30) Votava, O.; Kassi, S.; Campargue, A.; Romanini, D. Comb coherence-transfer and cavity ring-down saturation spectroscopy around 1.65 μm: kHz-accurate frequencies of transitions in the $2\nu_3$ band of $^{12}CH_4$. *Phys. Chem. Chem. Phys.* **2022**, *24*, 4157−4173.

(31) Kassi, S.; Stoltmann, T.; Casado, M.; Daëron, M.; Campargue, A. Lamb dip CRDS of highly saturated transitions of water near 1.4 μm. *J. Chem. Phys.* **2018**, *148*, No. 054201.

(32) Bielska, K.; Cygan, A.; Konefał, M.; Kowzan, G.; Zaborowski, M.; Charczun, D.; Wójtewicz, S.; Wcisło, P.; Masłowski, P.; Ciuryło, R.; et al. Frequency-based dispersion Lamb-dip spectroscopy in a high finesse optical cavity. *Opt. Express* **2021**, *29*, 39449−39460.

(33) Hartmann, J.-M. A simple empirical model for the collisional spectral shift of air-broadened CO_2 lines. *Journal of Quantitative Spectroscopy and Radiative Transfer* **2009**, *110*, 2019−2026.

(34) Twagirayezu, S.; Hall, G. E.; Sears, T. J. Frequency measurements and self-broadening of sub-Doppler transitions in the $\nu_1+\nu_3$ band of C_2H_2. *J. Chem. Phys.* **2018**, *149*, No. 154308.

(35) Tan, Y.; Hua, T.-P.; Tang, J.-D.; Wang, J.; Liu, A.-W.; Sun, Y. R.; Cheng, C.-F.; Hu, S.-M. Self- and N_2-broadening of CO in the low-pressure regime. *J. Phys. Conf. Ser.* **2023**, *2439*, No. 012007.

(36) Ma, L.-S.; Ye, J.; Dubé, P.; Hall, J. L. Ultrasensitive frequency-modulation spectroscopy enhanced by a high-finesse optical cavity: theory and application to overtone transitions of C_2H_2 and C_2HD. *Journal of the Optical Society of America B* **1999**, *16*, 2255−2268.

(37) Aiello, R.; Di Sarno, V.; Santi, M. G. D.; De Rosa, M.; Ricciardi, I.; Giusfredi, G.; De Natale, P.; Santamaria, L.; Maddaloni, P. Lamb-dip saturated-absorption cavity ring-down rovibrational molecular spectroscopy in the near-infrared. *Photonics Research* **2022**, *10*, 1803−1809.

(38) Cazzoli, G.; Dore, L.; Cludi, L.; Puzzarini, C.; Beninati, S.; et al. Hyperfine structure of J= 1 ≤ ftarrow 0 transition of ^{13}CO. *J. Mol. Spectrosc.* **2002**, *215*, 160−162.

(39) Fleurbaey, H.; Čermák, P.; Campargue, A.; Kassi, S.; Romanini, D.; Votava, O.; Mondelain, D. $^{12}CO2$ transition frequencies with kHz-accuracy by saturation spectroscopy in the 1.99−2.09 μm region. *Phys. Chem. Chem. Phys.* **2023**, *25*, 16319−16330.

(40) Miller, C. E.; Montgomery, M. A.; Onorato, R. M.; Johnstone, C.; McNicholas, T. P.; Kovaric, B.; Brown, L. R. Near infrared

spectroscopy of carbon dioxide. II: $^{16}O^{13}C^{16}O$ and $^{16}O^{13}C^{18}O$ line positions. *J. Mol. Spectrosc.* **2004**, *228*, 355−374.

(41) Perevalov, B. V.; Perevalov, V. I.; Campargue, A. A (nearly) complete experimental linelist for $^{13}C^{16}O_2$, $^{16}O^{13}C^{18}O$, $^{16}O^{13}C^{17}O$, $^{13}C^{18}O2$ and $^{17}O^{13}C^{18}O$ by high-sensitivity CW-CRDS spectroscopy between 5851 and 7045 cm^{-1}. *Journal of Quantitative Spectroscopy and Radiative Transfer* **2008**, *109*, 2437−2462.

(42) Ibrahim, M. T. I.; Alatoom, D.; Furtenbacher, T.; Császár, A. G.; Yurchenko, S. N.; Azzam, A. A.; Tennyson, J. MARVEL analysis of high-resolution rovibrational spectra of $^{13}C^{16}O_2$. *J. Comput. Chem.* **2024**, DOI: 10.1002/jcc.27266.